

3D-QSAR studies of pyruvate dehydrogenase kinase inhibitors based on a divide and conquer strategy[☆]

Teshome Leta Aboye, M. Elizabeth Sobhia and Prasad V. Bharatam^{*}

Department of Medicinal Chemistry, National Institute of Pharmaceutical Education and Research (NIPER), Sector-67,
S.A.S. Nagar (Mohali) 160062, India

Received 23 January 2004; revised 5 March 2004; accepted 5 March 2004

Available online 12 April 2004

Abstract—PDHK is a highly specific enzyme, which inhibits PDC thereby reducing the conversion of pyruvate to AcetylCoA leading to increased glucose and lactate level contributing to various pathological disease states. 3D-QSAR CoMFA studies were performed on diverse PDHK inhibitors based on maximum common substructural alignments of different classes of molecules with the selected reference molecule using a divide and conquer strategy. Statistically robust CoMFA model was obtained with a cross-validated correlation coefficient of 0.561 and conventional correlation coefficient of 0.990. Predictive correlation coefficient r^2_{pred} was found to be 0.875.

© 2004 Elsevier Ltd. All rights reserved.

1. Introduction

Pyruvate dehydrogenase kinases (PDHK) are a group of highly specific enzymes, which deactivate pyruvate dehydrogenase complex (PDC) and hence impair carbohydrate metabolism by reducing the oxidation of pyruvate. PDC catalyzes the irreversible conversion of pyruvate to acetyl-CoA,¹ which then proceeds to oxidation through the tricarboxylic acid (TCA) cycle or conversion to fatty acids for storage.² The flux through this complex is controlled by the phosphorylation state of three seryl residues located on the α chain of E1 subunit of pyruvate dehydrogenase (E1).³ ATP dependent phosphorylation of a specific residue of the E1 by PDHK leads to inactivation, and dephosphorylation by phosphatases reactivates the PDC complex (Fig. 1). At least four distinct binding sites of PDHK have been identified, comprising (1) the ATP binding site on the catalytic domain, (2) the putative binding site of the lipoyl domain of the E2 component of the PDC, (3) an allosteric binding site and (4) the DCA binding site. The crystal structure study performed using engineered version of human PDHK2 has shown that the binding pocket of PDHK2 is predominantly hydrophobic. Even though, the structures of human PDHK2 in complex

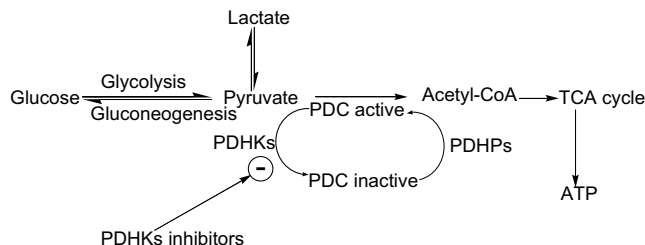


Figure 1. Regulation of PDC activity by interconversion between active and inactive forms.

with synthetic compounds were determined at various binding sites, the coordinates of these complexes are not yet made public.⁴

The activity of the PDC is lower during conditions of reduced oxidative glucose metabolism such as diabetes, obesity, and starvation and in patients with congenital lactic acidosis.⁵ When glucose and insulin levels are high, the serine residues are dephosphorylated by an active pyruvate dehydrogenase phosphatase, which results in an active complex and the flow of energy from glycolysis to oxidation or storage. In diabetes, the PDHK is activated, resulting in phosphorylation and inactivation of the E1 subunit of PDC.⁵ This serves to preserve the three-carbon skeleton of the pyruvate for gluconeogenesis, which maintains serum glucose levels but also contributes to pathologic hyperglycemia in

[☆] NIPER communication number 261.

^{*} Corresponding author. Tel.: +91-172-2214684; fax: +91-172-22146-92; e-mail: pvbharatam@niper.ac.in

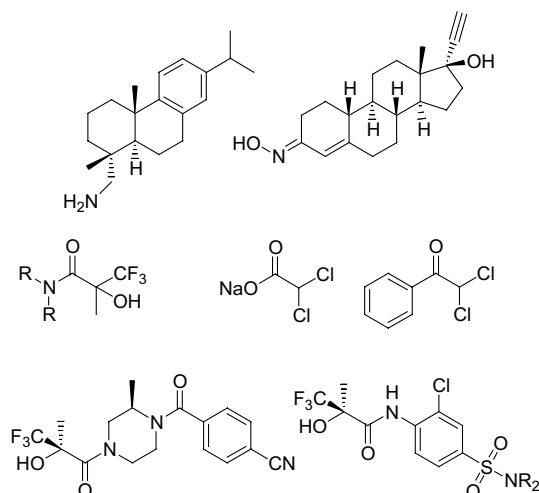


Figure 2. PDHK inhibitors.

diabetes.² Hence, restoring the normal activity of PDC through inhibition of PDHK can alleviate the associated pathological diseases including hyperglycemia in diabetes.

It has been reported that diverse classes of compounds (Fig. 2) can act as inhibitors of PDHK.^{5–9} The structural diversity of PDHK inhibitors suggests that compounds with different pharmacophores may interact with PDHK binding sites. Dichloroacetate (DCA) is a known inhibitor of PDHK, which can lower the plasma lactate, alanine and glucose levels in diabetic patients.¹⁰ DCA has proven efficacy as a therapy for diabetes, ischemia, endotoxic shock, lactic acidosis and cardiac insufficiency. However, DCA is associated with toxicity such as neuropathic effects, cataractic formation and testicular degeneration.⁶ Diverse amides of (*R*)-3,3,3-trifluoro-2-hydroxy-2-methylpropionic acid derivatives are the first inhibitors of PDHK reported without halogens α , to a carbonyl group, which is much more potent than the dichloroacetate in primary enzymatic assay and orally bioavailable.⁵ Structure–activity relationships of the secondary amides of (*R*)-3,3,3-Trifluoro-2-hydroxy-2-methylpropionic acid derivative have shown that (*R*)-3,3,3-trifluoro-2-hydroxy-2-methyl moiety is an optimum group for PDHK inhibition and methyl substitution on the piperazine ring at the 2- and 5-position (with *S* and *R* absolute stereochemistry) markedly

increased the biological activity of the compounds.⁶ In order to have further insights into the structural requirements of these compounds as PDHK inhibitors, we performed three-dimensional quantitative structure–activity relationships (3D-QSAR) using comparative molecular field analysis (CoMFA).¹¹ CoMFA, known for the renowned robustness of the model it produces, has been used regularly to produce the 3D models to indicate the regions that affect the biological activity with a change in the chemical substitution.^{12–15} CoMFA models can describe the relative changes in magnitude of the steric and electrostatic fields as a function of the sampled compounds chosen from dataset.

2. Computational details

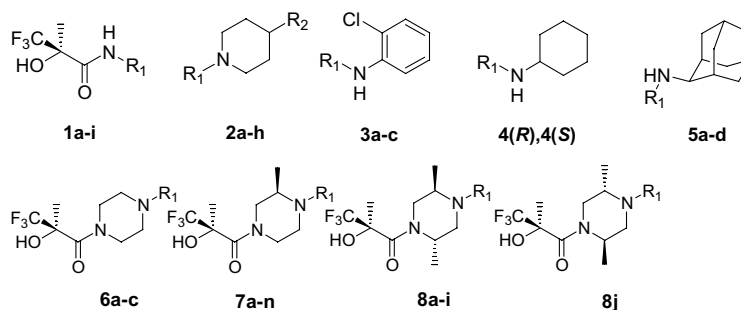
2.1. Dataset for analysis

Reported in vitro biological activity data (IC_{50} in primary enzymatic assay of PDHK inhibition) on two series of amides of (*R*)-3,3,3-trifluoro-2-hydroxy-2-methylpropionic acid derivatives,^{5,6} were used in the study (Scheme 1, Table 1). The molecules for which stereochemistry were not explicitly defined were excluded from the present work. Those molecules, which do not have exact biological activity value in numerical form, were also excluded from the analysis. Range of biological activity used for the analysis was about 5 log units (i.e., pIC_{50} 3.38–8.48). IC_{50} values were converted into pIC_{50} according to the formula.

$$pIC_{50} = -\log IC_{50}$$

2.2. Molecular modelling

All molecular modelling studies were performed using the molecular modelling package SYBYL6.9¹⁶ installed on a Silicon Graphics Octane2 Work station. Since the crystal structure of PDHK–inhibitor complex is not available the lowest energy conformer of the most active molecule for which some information is available from European patent EP 1247860 about the binding conformation was used as bioactive conformation.⁴ **8d**, that is, the molecule having highest EC_{50} in cellular assay of increased oxidation of lactate, was subjected to systematic conformational search with 15° increments followed by further geometry optimisation using



Scheme 1. Structures of molecules used in the CoMFA analysis and their PDHK inhibitory activity (IC_{50}).

Table 1. The IC₅₀ values of the set of molecules employed in this study, the structures of the molecules in this table are given in Scheme 1

Sr. no.	Mole- cule	R ₁	R ₂	IC ₅₀ (μM)
1	1a	Ph	—	35
2	1b	4-(PhCO)Ph	—	9.3
3	1c	4-[SO ₂ (1-piperidine)]Ph	—	9.3
4	1d	2-Cl-4-(SO ₂ F)Ph	—	0.077
5	1e	2-Cl-4-(PhCO)Ph	—	0.11
6	1f	2-Cl-4-(CO ₂ Me)Ph	—	0.12
7	1g	2-Cl-4-(CO ₂ H)Ph	—	0.090
8	1h	2-Cl-4-[CO(1-piperidine)]Ph	—	1.50
9	1i	2-Cl-4-[SO ₂ (1-piperazine)]Ph	—	0.055
10	2a	CONHMe	Bn	22.4
11	2b	CONMe ₂	Bn	416
12	2c	COMe	Bn	74
13	2d	CO t -Bu	Bn	282
14	2e	COC(OH)(CH ₃) ₂	Bn	150
15	2f	COC(OH)(c -Pr)	Bn	260
16	2g	COCCl ₃	Bn	30
17	2h(R)	R-COC(CF ₃)(OH)Me	Pr	3.1
18	2h(S)	S-COC(CF ₃)(OH)Me	Pr	75
19	3a(R)	R-COC(CF ₃)(OH)Me	—	0.300
20	3a(S)	S-COC(CF ₃)(OH)Me	—	9.8
21	3b	COC(Me)(OH)Me	—	5.0
22	3c	COCHCl ₂	—	47
23	4(R)	R-COC(CF ₃)(OH)Me	—	6.2
24	4(S)	S-COC(CF ₃)(OH)Me	—	200
25	5a(R)	R-COC(CF ₃)(OH)Me	—	0.30
26	5a(S)	S-COC(CF ₃)(OH)Me	—	11
27	5b	COC(Me)(OH)Me	—	10
28	5c	COC(CF ₃) ₂ (OH)	—	17
29	5d	COC(OH)(c -Pr)	—	15
30	6a	Bn	—	19.9
31	6b	4-NC(C ₆ H ₄)CO	—	6.7
32	6c	4-NO ₂ -2-pyridyl	—	2.84
33	7a	PhCO	—	0.173
34	7b	PhSO ₂	—	0.037
35	7c	4-NC(C ₆ H ₄)CO	—	0.079
36	7d	PhOC(NCN)	—	0.049
37	7e	4-PhCO(C ₆ H ₄)CO	—	0.034
38	7f	CBZ	—	0.021
39	7g	c -HexCO	—	0.064
40	7h	4-NO ₂ -2-pyridyl	—	0.112
41	7i	1-naphthoyl	—	0.070
42	7j	3,4,5-tri-OMe(C ₆ H ₂)CO	—	0.040
43	7k	SO ₂ -1-naphth	—	0.025
44	7l	2,4,6-tri-Me(C ₆ H ₂)PhSO ₂	—	0.039
45	7m	3,5-di-Cl(C ₆ H ₃)CO	—	0.028
46	7n	4- t -Bu(C ₆ H ₄)SO ₂	—	0.036
47	8a	Bn	—	0.082
48	8b	SO ₂ -1-naphth	—	0.0045
49	8c	3,5-di-Cl(C ₆ H ₃)CO	—	0.0033
50	8d	4-NC(C ₆ H ₄)CO	—	0.016
51	8e	PhOC(NCN)	—	0.0091
52	8f	4-MeO ₂ C(C ₆ H ₄)CO	—	0.019
53	8g	4-PhCO(C ₆ H ₄)CO	—	0.0198
54	8h	CBZ	—	0.0143
55	8i	c -HexCO	—	0.013
56	8j	SO ₂ -1-naphth	—	49

MOPAC¹⁷ interfaced with SYBYL. The AM1 Hamiltonian was employed in energy minimisation and charge calculations. The global minimum conformer obtained was taken as template and rest of the molecules were built from it. The following specific software options were employed while performing AM1 studies: conver-

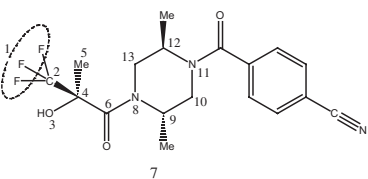
gence = precise, optimisation = full, keyword = mmok. The atomic point charges were calculated by the Mulliken method, as included in the MOPAC-AM1 studies. The conformations of the molecules with the piperazine central unit have been modelled according to the conformational preferences mentioned by Aicher et al.⁶ Also, the structure with *syn* arrangement were employed in the study as desirable. Our studies using AM1 method clearly showed that the *syn* arrangement is more preferred by about 0.2 kcal/mol in this series of molecules.

2.3. Alignment of molecules

The alignment, that is, molecular orientation is one of the most sensitive input areas for 3D-QSAR studies.^{11,18} In the absence of any 3D information on the structure of the receptor, array of common chemical features encourages the study of the 3D structural requirements at the receptor. This may provide an advantageous starting point for the rational design of new inhibitors as well as to understand the existing structure–activity relationships (SAR). The present study is based upon the limited availability of the receptor structural information and the knowledge of the structurally diverse PDHK inhibitors. In these sets of molecules, since they are structurally diverse, the alignment of molecules could not be achieved by using any common alignment procedures. Hence, a divide and conquer strategy was employed. The alignment was achieved as follows: the molecules were first clustered into five structural classes for the purpose of maximum alignment. Each of these classes of molecules was independently superimposed onto the template molecule (**8d**) by ALIGN DATA-BASE option in SYBYL using the maximum substructure common for the respective class with template. Molecules in class V, which were not aligned properly by the above method, were manually aligned with the template using FIT ATOM command. Finally all the five classes of aligned molecules were combined for the QSAR analysis (CoMFA). Scheme 2 shows the structural classes and substructures used for the alignment. The total aligned molecules are shown in Figure 3.

2.4. CoMFA interaction energies

The steric and electrostatic CoMFA potential fields were calculated at each lattice intersection of a regularly spaced grid of 2.0 Å. The grid box dimensions were determined automatically in such a way that the region boundaries were extended beyond 4 Å in each direction from the co-ordinate of each molecule. The van der Waals potential and Coulombic terms, which represent steric and electrostatic fields, respectively, were calculated using the standard Tripos force fields. A distance-dependent dielectric constant of 1.00 was used. An sp³ hybridised carbon atom with +1 charge served as probe atom to calculate steric and electrostatic fields. The steric and electrostatic contributions were truncated to +30.0 kcal/mol and electrostatic contributions were ignored at the lattice intersections with maximal steric interactions.



Class (Alignment)	Substructure (Non-hydrogen atom numbers)	Molecules	No. of molecules
I	1-13	6a-c, 7a-7n, 8a-8j	27
II	2, 4-8, 13	1a-1i, 2d, 2e, 2h(R), 3a(R), 3b, 4(R), 5a(R), 5b, 5c	18
III	1, 2, 4, 6-8, 13	2h(S), 3a(S), 4(S), 5a(S)	4
IV	3-8, 13	2f, 5d	2
V	Fit atom alignment	2a, 2b, 2c, 2g, 3c	5

Scheme 2. Classes of aligned molecules.

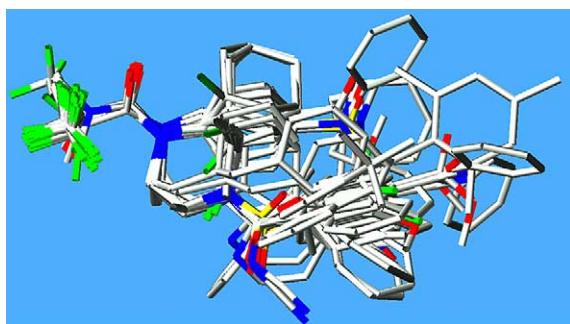


Figure 3. Aligned molecules.

included with training set for alignment as described above, and their activities were predicted using the model generated by the training set. The predictive correlation (r^2_{pred}), based on the test set molecules, is defined as

$$r^2_{\text{pred}} = (\text{SD-PRESS})/\text{SD}$$

where SD is the sum of the squared deviations between the biological activities of the test set and mean activities of the training set molecules and PRESS is the sum of squared deviation between predicted and actual activity values for every molecule in test set.

2.5. Partial least square (PLS) analysis

PLS method¹⁹ was used to linearly correlate the CoMFA fields to biological activity values. The cross-validation analysis was performed using leave-one-out (LOO) method in which one compound is removed from the dataset and its activity is predicted using the model derived from the rest of the dataset. The cross-validated r^2_{cv} that resulted in optimum number of components and lowest standard error of prediction were taken. Equal weights for CoMFA were assigned to steric and electrostatic fields using CoMFA_STD scaling option. To speed up the analysis and reduce noise, a minimum column filter value (σ) of 2.00 kcal/mol was used for the cross-validation. Final analysis (non-cross-validation) was performed to calculate conventional r^2 (r^2_{ncv}) using the optimum number of components. To further assess the robustness and statistical confidence of the derived model, bootstrapping analysis for 100 runs was performed.²⁰

2.6. Predictive correlation coefficient (r^2_{pred})

The predictive ability of the 3D QSAR model was determined from a set of eleven compounds that were not included in the training set. These molecules were

3. Results and discussion

The 3D QSAR CoMFA analysis was based on the superposition of structurally diverse compounds. The main difficulty in the development of reliable alignments²¹ is not only flexibility of most inhibitors but also the ambiguity of the receptor–ligand interactions.²² In spite of these difficulties, the statistically robust model was obtained employing maximum common substructural alignment of each class with the template molecule.

Summary of PLS analyses are shown in Table 2. The actual and predicted pIC_{50} values for training and test set are shown in Tables 3 and 4, respectively. The CoMFA steric and electrostatic fields for the analysis are presented as contour plots in Figures 4 and 5, respectively. The most active molecule (**8c**) is shown in the background of the contour maps to aid in visualisation. The plot of actual and predicted pIC_{50} of the training set and a histogram of the residuals of test set molecules are shown in Figures 6 and 7, respectively.

The molecules were randomly divided into training and test sets. The model developed based on 45 molecules in the training set and 11 molecules in the test set exhibited a cross-validated coefficient of 0.561 with the standard

Table 2. Summary of PLS analysis

Statistical parameters	
PRESS	1.070
r_{cv}^2	0.561
N	8
SEE	0.159
r_{ncv}^2	0.990
F -test value	459.446
r_{bs}^2	0.995
SD	0.002
Prob. of $r^2 = 0$	0.000
r_{pred}^2	0.875
<i>Fraction of field contributions</i>	
Steric	0.432
Electrostatic	0.568

PRESS = Predictive residual sum of squares of training set; N = no. of components; r_{cv}^2 = cross-validated coefficient; r_{ncv}^2 = conventional correlation coefficient; SEE = standard error of estimate; r_{pred}^2 = predictive correlation coefficient, r_{bs}^2 = correlation coefficient after 100 runs of bootstrapping, SD = standard deviation from 100 bootstrapping runs.

error of 0.159 and optimum number of components of 8. Non-cross-validated correlation coefficient of 0.990 was obtained using the optimum number of components of 8. The contributions of the steric and electrostatic fields were obtained in the ratio of ~0.4:0.6. To test the predictive ability of the resulting model, a test set of 11 molecules excluded from the model derivation was used whereby the predictive correlation coefficient r_{pred}^2 of 0.875 was obtained. This indicates the robust predictive ability of the model. A high r^2 value (0.995) of 100 runs of bootstrapping supports the statistical validity of the model.

The QSAR produced by a CoMFA model, with its hundreds or thousands of terms, is usefully represented as a three-dimensional ‘coefficient contour’ maps.¹¹ In general, the contour maps surround all lattice points where the QSAR strongly associates changes in the molecular field values with changes in binding affinity. More specifically, the polyhedra surround lattice points where the scalar products of the associated QSAR coefficient and the standard deviation of all values in the corresponding column (STDEVXCOEFF) of the data table are higher or lower than a user-specified value. Figures 4 and 5 show contour maps, for steric and electrostatic interactions, respectively. Green contours show the points where sterically bulkier groups are associated with increase in biological activity whereas the yellow contours highlight the points where such bulkier groups may lower biological activity (Fig. 4). Two green contours are observed near two methyl groups (one above the plane of 5-(*R*)-methyl group while the other below the plane of 2-(*S*)-methyl group substituted on the piperazine ring) of the most active molecule indicating preference for bulkier substituent at these positions. The orientations of these two methyl groups substituted on the piperazine ring were reported to play an important role in biological activity.⁵ The more potent molecules have one (**7b–g**, **7i–n**) or both (**8a–e**) methyl substituents on the piperazine ring proximal to the green contours. In general, less active

Table 3. Actual and predicted inhibitory activities (pIC₅₀) of the training set molecules

Sr. no.	Molecule	Actual pIC ₅₀	Predicted pIC ₅₀	Residual
1	6a	4.70	4.89	–0.19
2	6b	5.17	5.34	–0.17
3	6c	5.55	5.47	0.08
4	7a	6.76	7.02	–0.26
5	7b	7.43	7.37	0.06
6	7c	7.10	6.72	0.38
7	7d	7.31	7.31	0
8	7e	7.47	7.56	–0.09
9	7g	7.19	7.11	0.08
10	7h	6.95	6.94	0.01
11	7i	7.15	7.12	0.03
12	7j	7.40	7.468	–0.07
13	7k	7.60	7.75	–0.15
14	7l	7.41	7.32	0.09
15	7n	7.44	7.31	0.13
16	8a	7.09	7.18	–0.09
17	8b	8.35	8.28	0.07
18	8c	8.48	8.54	–0.06
19	8d	7.79	7.78	0.01
20	8g	7.70	7.66	0.04
21	8h	7.84	7.85	–0.01
22	8j	4.31	4.43	–0.12
23	1b	5.03	4.95	0.08
24	1c	5.03	5.28	–0.25
25	1d	7.11	7.24	–0.13
26	1e	6.96	7.01	–0.05
27	1f	6.92	6.87	0.05
28	1g	7.05	6.99	0.06
29	1i	7.26	6.89	0.37
30	2a	4.65	4.45	0.2
31	2b	3.38	3.20	0.18
32	2d	3.55	3.61	–0.06
33	2e	3.82	3.89	–0.07
34	2g	4.52	4.60	–0.08
35	2h(R)	5.51	5.53	–0.02
36	2h(S)	4.12	4.01	0.11
37	3a(R)	6.52	6.78	–0.26
38	3a(S)	5.01	4.82	0.19
39	3c	4.33	4.29	0.04
40	4(R)	5.21	5.30	–0.09
41	4(S)	3.70	3.76	–0.06
42	5a(R)	6.52	6.35	0.17
43	5a(S)	4.96	5.16	–0.2
44	5b	5.00	4.94	0.06
45	5c	4.77	4.80	–0.03

Table 4. Actual and predicted inhibitory activities (pIC₅₀) of the test set of molecules

Sr. no.	Molecule	Observed pIC ₅₀	Predicted pIC ₅₀	Residual
1	7f	7.68	7.24	0.45
2	7m	7.55	7.15	0.4
3	8e	8.04	7.63	0.41
4	8f	7.72	7.20	0.52
5	8i	7.89	7.74	0.15
6	1a	4.46	5.95	–1.49
7	1h	5.82	6.22	–0.4
8	2c	4.13	4.13	0
9	2f	3.58	3.52	0.06
10	3b	5.30	5.07	0.23
11	5d	4.82	4.16	0.66

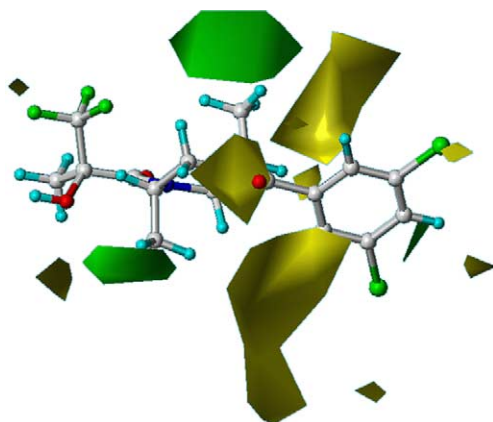


Figure 4. CoMFA STDEVXCOEFF steric contour maps. The most active molecule is displayed in the background.

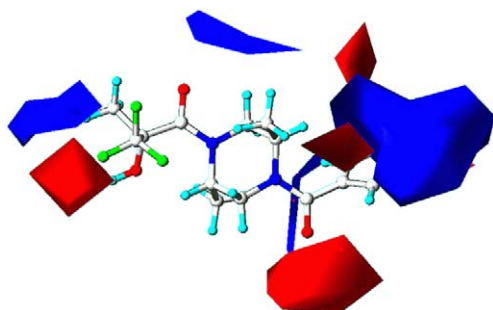


Figure 5. CoMFA STDEVXCOEFF electrostatic contour maps. The most active molecule is displayed in the background.

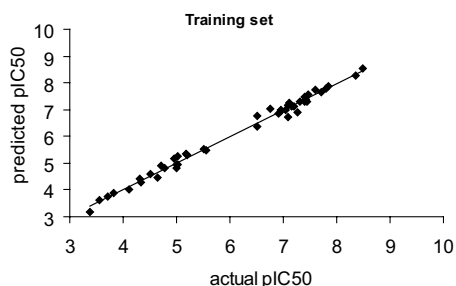


Figure 6. Plot of actual versus predicted pIC_{50} of the training set molecules.

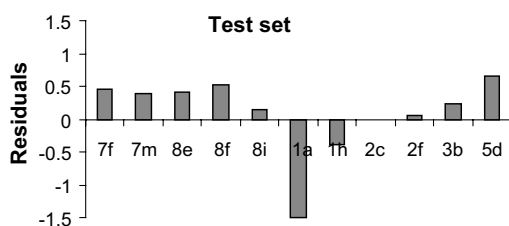


Figure 7. Histogram of residuals of the test set molecules.

molecules had bulkier group(s) proximal to the sterically ‘forbidden’ yellow contours. These yellow contours are observed above and below the plane of phenyl ring of the most active molecule each of them at the close proximity of the respective nearby green contour that is observed near 2-(*S*) and 5-(*R*) methyl groups. The relatively lower activity of **6a**, **6c** and **8j** despite structural similarity to subseries **7** and subseries **8** can be due to embedment of the bulkier phenyl ring for **6a**, naphthyl ring for **8j** and pyridine ring for **6c** in one of the sterically ‘forbidden’ yellow region that was observed around aromatic ring of the most active molecule. Most of the molecules in the subseries **2** have either phenyl or propyl group significantly embedded in the yellow sterically ‘forbidden’ zone, which may be responsible for their lower activity. The more potency of **7c** as compared to **6b** is due to the presence of (*R*)-methyl substituent on the piperazine ring in **7c** that is oriented at sterically favourable region but is absent in **6b**. Furthermore, **8d** is more potent than **7c** due to the presence of both methyl substituents on the piperazine ring that are oriented at the sterically favourable green regions.

In electrostatic contour maps (Fig. 5), red contours indicate where more electronegative groups associated with increase in biological activity. They are observed near the trifluoro group and one red contour near (C_6H_5)CO carbonyl oxygen atom and three more red contours around the aromatic ring of the most active molecule (**8c**), which is also common in other highly active molecules. Blue contours show regions that are favourable for more electropositive groups (Fig. 5). Blue contours are observed proximal to methyl group of trifluoro-2-hydroxy-2-methylpropanamide and near C6 carbon of piperazine ring. A big blue contour is also observed enclosing partly the aromatic ring and extending to piperazine ring being surrounded by the smaller red contours and further extended to the red contour proximal to the (C_6H_5)CO carbonyl oxygen atom. More active molecules had fluorine or trifluoro group in close proximity of red contour and another red contour near oxygen of 4-N-SO₂ (**11d**, **11m**, **11n**, **11p**, **14c**, **3d**, **3e**), near oxygen atom of 4-N-CO (**7a**, **7c**, **7e**, **7g**, **7i**, **7j**, **7m**, **8c**, **8d**, **8f**, **8g**, **8h**, **8i**) and near nitrogen atoms of C(NCN) (**7d**), which may account for their higher biological activity. Less active molecules had more electronegative groups such as chlorine of trichloro group (**2g**), fluorine of trifluoro group (**5c**), fluorine of SO₂F (**1c**) and nitro group (**6c**) embedded in the blue contour. The more potency of *R*-stereoisomer as compared to *S*-stereoisomer (**2h(R)** versus **2h(S)**, **3a(R)** and **3a(S)**, **4(R)** versus **4(S)**, and **5a(R)** versus **5a(S)**) is because of the disposition of the electron rich substituent, the trifluoro group and electropositive group, methyl at electrostatically unfavourable blue and red contour maps, respectively, in *S*-stereoisomer. Overall, the most active molecules had both bulkier and more electronegative groups or at least one of them properly oriented, respectively, at the sterically and electrostatically favourable region(s).

The CoMFA model is usually expected to poorly predict compounds with unique structural modification. Hence,

it is not surprising that **1a**, the only group containing phenyl group, and **5d**, the only molecule having cyclopropyl moiety substituted on propanamide moiety in the respective congeneric series, is not well predicted by the model.

4. Conclusions

In the absence of any 3D structural information of the receptor, it is important to obtain model accounting for 3D structural requirements at the receptor. This model may be useful to prioritise molecules for synthesis or identify and computationally screen novel scaffolds. The present work focuses on use of QSAR CoMFA methodology to develop predictive model for the structurally diverse PDHK inhibitors. The model developed in the present study is robust despite diversity of compound series used for the analysis. The analyses of the orientations of the molecules around the contours have led to interesting conclusions about the different functional groups on biological activity. These information is useful in guiding the design of novel and more active compounds in this series. The model so generated is also consistent with literature report that (*R*)-3,3,3-trifluoro-2-hydroxy-2-methyl moiety is an optimum group for PDHK inhibition and the 2-(*S*) and 5-(*R*)-methyl substituents on the piperazine ring would enhance biological activity of the molecules.

References and notes

- Patel, M. S.; Roche, T. E. *FASEB J.* **1990**, *4*, 3224–3233.
- Randle, P. J. *Biochem. Soc. Trans.* **1986**, *14*, 799–806.
- Stepp, L. R.; Pettit, F. H.; Yeaman, S. J.; Reed, L. J. *J. Biol. Chem.* **1983**, *258*, 9454–9458.
- Knoechel, T. R.; Robinson, C. M.; Taylor, W. E.; Tucker, A. D. European Patent 1,247,860, 2002.
- Aicher, T. D.; Anderson, R. C.; Rebernitz, G. R.; Copola, G. M.; Jewell, C. F.; Knorr, D. C.; Liu, C.; Sperbeck, D. M.; Brand, L. J.; Strohschein, R. J.; Gao, J.; Vinluan, C. C.; Shetty, S. S.; Dragland, C. J.; Kaplan, E. L.; Delgrande, D.; Islam, A.; Liu, X.; Lozito, R. J.; Maniara, W. M.; Walter, R. E.; Mann, W. R. *J. Med. Chem.* **1999**, *42*, 2741–2746.
- Aicher, T. D.; Anderson, R. C.; Gao, J.; Shetty, S. S.; Copola, G. M.; Stanton, J. L.; Knorr, D. C.; Sperbeck, D. M.; Brand, L. J.; Vinluan, C. C.; Kaplan, E. L.; Dragland, C. J.; Tomaselli, H. C.; Islam, A.; Lozito, R. J.; Liu, X.; Maniara, W. M.; Fillers, W. S.; Delgrande, D.; Walter, R. E.; Mann, W. R. *J. Med. Chem.* **2000**, *43*, 236–249.
- Rebernitz, G. R.; Aicher, T. D.; Stanton, J. L.; Gao, J.; Shetty, S. S.; Knorr, D. C.; Strohschein, R. J.; Tan, J.; Brand, L. J.; Liu, C.; Wang, W. H.; Vinluan, C. C.; Kaplan, E. L.; Dragland, C. J.; Delgrande, D.; Islam, A.; Lozito, R. J.; Liu, X.; Maniara, W. M.; Mann, W. R. *J. Med. Chem.* **2000**, *43*, 2248–2257.
- Aicher, T. D.; Damon, R. E.; Koletar, J.; Vinluan, C. C.; Brand, L. J.; Gao, J.; Shetty, S. S.; Kaplan, E. L.; Mann, W. R. *Bioorg. Med. Chem. Lett.* **1999**, *9*, 2223–2228.
- Espinal, J.; Leesnitzer, T.; Hassman, A.; Beggs, M.; Cobb, J. *Drug Dev. Res.* **1995**, *35*, 130–135.
- Stacpoole, P. W.; Moore, G. W.; Kornhauser, D. M. *N. Engl. J. Med.* **1978**, *298*, 526–530.
- Cramer, R. D., III; Patterson, D. E.; Bunce, J. D. *J. Am. Chem. Soc.* **1988**, *110*, 5959–5967.
- Desiraju, G. R.; Sarma, J. A.; Raveendra, D.; Gobalakrishnan, B.; Thilagavathi, R.; Sobhia, M. E.; Subramanya, H. S. *J. Phys. Org. Chem.* **2001**, *14*, 481–487.
- Desiraju, G. R.; Gobalakrishnan, B.; Jetti, R. K.; Nagaraju, A.; Raveendra, D.; Sarma, J. A.; Sobhia, M. E.; Thilagavathi, R. *J. Med. Chem.* **2002**, *45*, 4847–4857.
- Amrose, A. E.; Welsh, W. J. *J. Med. Chem.* **2001**, *44*, 3849–3855.
- Chakraborti, A. K.; Gobalakrishnan, B.; Sobhia, M. E.; Malde, A. *Bioorg. Med. Chem. Lett.* **2003**, *13*, 1403–1408.
- SYBYL6.9, Tripos Associates Inc.: 1699, S Hanley Rd., St. Louis, MO63144, USA.
- Dewar, M. J. S.; Zoebisch, E. G.; Healy, E. F.; Stewart, J. J. P. *J. Am. Chem. Soc.* **1985**, *107*, 3902–3909.
- Kim, K. H. In *Molecular Similarity in Drug Design*; Dean, P. M., Ed.; 1st ed.; Blackie Academic and Professional: Glasgow, 1995; pp 303–305.
- Cramer, R. D.; Bunce, J. D.; Patterson, D. E. *Quant. Struct.-Act. Relat.* **1988**, *7*, 18–25.
- Chakraborti, A. K.; Gobalakrishnan, B.; Sobhia, M. E.; Malde, A. *Eur. J. Med. Chem.* **2003**, *38*, 975–982.
- Zwaagstra, M. E.; Timmerman, H.; van de Stoppel, A. C.; de Kanter, F. J. J.; Tamura, M.; Wada, Y.; Zhang, M. Q. *J. Med. Chem.* **1998**, *41*, 1428–1438.
- Zhang, M. Q.; Zwaagstra, M. E.; Nederkoorn, P. H. J.; Timmerman, H. *Bioorg. Med. Chem. Lett.* **1997**, *7*, 1331–1336.